RESEARCH

Modelling of a 12-DoF Parachute–Riser–Payload system dynamics using Kane's method

Prashant G. Iyer[1]

Abstract

The dynamic behaviour of parachutes is highly complex and characterised by non-linear, time-dependant, Fluid–Structure Interactions, which is computationally intensive and hence not a viable option for incorporating into trajectory simulations. The paper describes modelling of a "Computationally efficient, High Fidelity Multi-Body" Parachute–Elastic Riser–Payload system, capable of simulating trajectory from parachute deployment to parachute separation. The matrix form of Kane's method is used to derive the kinematic and dynamic equations of motion for the system, which avoids the complications of symbolically deriving these equations. The developed model is validated with published literature results formulated using the Newton–Euler method and simulation results describing the typical trajectory and attitude of the system during the descent phase are presented.

Keywords Multi-body dynamics · Parachute–Riser–Payload system · Kane's method · Generalised coordinates · Parachute opening transients · Equations of motion

1 Introduction

Parachutes belong to the class of aerodynamic decelerators, serving the primary purpose of controlling the descent rate of any payload and ensuring a smooth and accurate landing. They are used in a wide variety of applications like skydiving, planet-probe landing, human-capsule recovery, aerial delivery of equipments and supplies, etc. [10]. A typical deceleration system for spacecraft recovery consists of a clustered parachute system comprising different kinds of parachutes, which deploy in a predetermined sequence to bring down the velocity of the spacecraft to safe levels at the instant of splash-down whilst maintaining the stability of the system [13].

Available literature like Fallon (1991) [2], Guglieri (2012) [4], Ibrahim and Engdahl (1974) [8] and Paul et al. (2016) [13], have modelled a multi-body Parachute Payload system using the Newton–Euler method with varying degrees of freedom and validated their model with actual flight data. However, this formulation involves deriving the internal constraint forces, which tends to become tedious when the complexity of the system increases,

✉ P.G. Iyer
prashant_gi@vssc.gov.in

1 Vikram Sarabhai Space Centre, Thiruvananthapuram, Kerala 695022, India

as in the case of a multi-chute system. On the other hand, analytical methods like the Euler–Lagrange method requires differentiation of a scalar Lagrangian function, which can become a laborious task for systems with higher degrees of freedom and can lead to the issue of *intermediate swell*, as reported by Duan (2006) [1]. Kane's method is widely used to model complex multi-body systems with high degrees of freedom, attributable to its use of generalised speeds. It results in a simplistic vectorial form of equations of motion involving partial velocity and accelerations, describing the system as a whole and eliminating the need to derive constraint forces and moments. Stoneking (2013) [16] presented a matrix formulation of Kane's equation for fixed-mass systems, which has a form more suitable for computers and that can be numerically solved in a faster and efficient manner [12]. However, matrix expressions to model variable-mass systems are not provided, which has been addressed in this paper.

Ke et al. (2009) [10] presented a generic algorithm to model and simulate the dynamics of any general parachute-payload configuration, including the parachute-opening transients and contact forces, using the analytical form of Kane's equation. During the phase of parachute deployment and inflation, the canopy shape as well as volume of trapped air inside the canopy increases quickly due to inflation, resulting in a change in drag as well as the overall CG of the parachute, which is not accurately modelled in Ke et al. (2009) [10]. However, modelling these processes with high fidelity is essential as maximum axial as well as lateral loads on the payload occurs in this phase, which is highly critical for human-capsule recovery missions.

This paper discusses the modelling of a Parachute–Riser–Payload System (PRPS) consisting of a rigid payload and a rigid parachute linked using an elastic riser having a non-zero mass using the matrix form of Kane's equation. This high-fidelity model is capable of simulating the parachute dynamics from parachute deployment till parachute separation, including the parachute-opening transients where the PRPS acts as a constant-mass system with variable-mass bodies. The variation in drag as well as parachute geometry during the parachute inflation are also accounted for and validated with flight results achieved from the payload-airdrop tests. Analytical expressions for fore-body wake effects and energy modifications due to apparent mass have also been included to make the model more realistic.

1.1 Notations

The list of notations used in this paper to represent various vector quantities and matrices is given in Table 1, following the standards used in Pal (2020) [12].

2 Kane's method for variable-mass systems

Hurtado (2018) derived the Lagrange–Cayley equations for variable-mass systems from first principles, considering the kinematic relationships due to mass variations [7]. For a variable-mass multi-body system, consisting of N_b rigid bodies with n degrees of freedom, the system dynamics in Kane's form is developed as a set of scalar equations following Kane and

Table 1 Notations

Notation	Description
$^{B}C^{A}$	Transformation matrix to transform vector from frame A to frame B
$^{C}\vec{\omega}^{A/B}$	Angular velocity of body A with respect to body B expressed in frame C
$^{C}\vec{\alpha}^{A/B}$	Angular acceleration of body A with respect to body B expressed in frame C
$^{C}\vec{r}^{P/n}$	Vector representing position of point P with respect to reference point n expressed in frame C
$^{C}\vec{v}^{P/n}$	Vector representing velocity of point P with respect to reference point n expressed in frame C
$^{C}\vec{a}^{P/n}$	Vector representing acceleration of point P with respect to reference point n expressed in frame C
$^{C}\vec{F}^{B}_{name}$	Force vector identified with *name* acting on body B expressed in the frame C
$^{C}\vec{M}^{B/o}_{name}$	Moment vector identified with *name* acting on body B about the point o, expressed in the frame C

Levison (1985) [9], extended from the Hurtado formulation using d'Alembert principle:

$$\sum_{k=1}^{N_b}\left[\vec{\omega}_r^k\cdot\left(\vec{M}_k-I_k\vec{\alpha}_k-\dot{I}_k\vec{\omega}_k-\vec{\omega}_k\times I_k\vec{\omega}_k\right)\right]+\sum_{k=1}^{N_b}\left[\vec{v}_r^k\cdot\left(\vec{F}_k-m_k\vec{a}_k-\dot{m}_k\vec{v}_k\right)\right]$$

$$+\sum_{k=1}^{N_b}\left[\sum_j\left(\vec{v}_{r,j}^k\cdot\left(\vec{f}_{j,k}-\dot{m}_{j,k}\vec{v}_{j,k}\right)\right)\right]=0, \tag{1}$$

$$r=1,2,\ldots,n,$$

where $\vec{F}_k$ and $\vec{M}_k$ are the active forces and moments acting on the kth body, respectively. $\vec{v}_r^k$ and $\vec{\omega}_r^k$ are the partial linear velocity and partial angular velocity of the kth body with respect to the rth generalised speed. $\vec{a}_k$ and $\vec{\alpha}_k$ are the linear and angular acceleration of the kth body, and $\vec{v}_k$ and $\vec{\omega}_k$ are the respective linear velocity and angular velocity of the CG. m_k defines the mass, and I_k defines inertia tensor of the kth body in its own body axis with respect to the CG [12]. $\vec{v}_{r,j}^k$ is the partial linear velocity of the ejected mass from the jth ejection location of kth body with respect to the rth generalised speed, $\vec{f}_{j,k}$ is the force acting on the jth ejected mass from the kth body and $\vec{v}_{j,k}$ is the inertial velocity of the jth ejected mass from the kth body.

Stoneking (2013) [16] styled the matrix form of Kane's formulation for a constant-mass rigid-body system. This is extended to include variable-mass effects, consistent with Equation (1) as

$$\left(\Omega^T[I]\Omega+V^T[m]V\right)\dot{u}=$$

$$\Omega^T\left(\{M\}-[I]\{\alpha_r\}-[\dot{I}]\{\omega\}-\{\omega\}\times[I]\{\omega\}\right) \tag{2}$$

$$+V^T\left(\{F\}-[\dot{m}]\{v\}-[m]\{a_r\}\right)+V_{EJ}^T\left(\{F_{EJ}\}-[\dot{M}_{EJ}]\{v_{EJ}\}\right),$$

where V and Ω are the partial linear and angular velocity matrices, a_r and α_r are the remainder linear acceleration and angular acceleration respectively, v and ω are the linear velocity and angular velocity vectors, F and M are the multi-body force and moment matrices, m and I are the multi-body mass and inertia matrices and $\vec{u}$ is column vector of generalised speeds, consistent with the nomenclature used by Stoneking (2013) [16]. V_{EJ} represents the
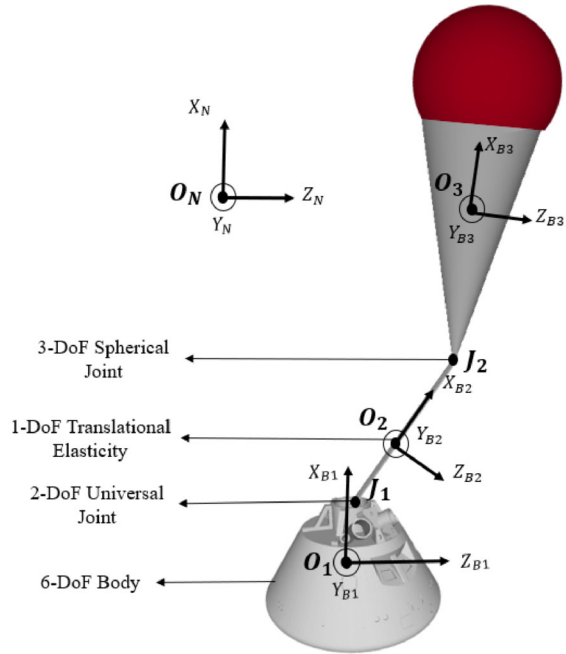
partial linear ejection velocity matrix, F_{EJ} is the ejected mass force matrix and M_{EJ} is the generalised multi-body ejection mass matrix.

V_{EJ} defined in Equation (2) is a 3-dimensional array, which can result in computationally intensive multiplication operation. Hence, a generalised reaction thrust generated as a direct consequence of mass variation is added in $\vec{M}_k$ and $\vec{F}_k$ matrices, as described in Ge et al. (1982) [3], simplifying Equation (2) as

$$
\left(\Omega^T [I] \Omega + V^T [m] V \right) \dot{u} =
$$
$$
\Omega^T \left(\{M\} - [I]\{\alpha_r\} - [\dot{I}]\{\omega\} - \{\omega\} \times [I]\{\omega\} \right) \tag{3}
$$
$$
+ V^T \left(\{F\} - [\dot{m}]\{v\} - [m]\{a_r\} \right).
$$

3 Mathematical modelling

3.1 Modelling of Parachute–Riser–Payload system

The 3-body PRPS presented in this paper is shown in Fig. 1, with O_1, O_2 and O_3 being the CGs of payload, riser and parachute, respectively. An elastic riser is connected to the payload (at the *riser attachment point*) on one end using a universal joint J_1 and to the parachute (at the *parachute confluence point*) on other end with a spherical joint J_2. From J_2, the suspension lines of the parachute fork out, with a semi-oblate spheroid canopy attached to it, forming the rigid-body parachute.

The following assumptions are considered while modelling the PRPS, consistent with the assumptions used in Ke et al. (2009) [10] and Fallon (1991) [2]:

- The surface area of the suspension lines and riser are considered small enough to neglect aerodynamic forces and moments.
- The forces due to twisting of the riser and suspension-line cables are considered negligible.
- Variation in parachute geometry and aerodynamic forces and moments due to distortion in the shape of the canopy are neglected.
- The aerodynamic centres of pressure remain on the axes of symmetry of the vehicle and the parachute, but do not necessarily coincide with the centres of mass of those bodies.
- Trajectory simulations are carried out considering the flat-Earth assumption.

3.2 Coordinate frames

The reference frames used in modelling the PRPS, as shown in Fig. 1, are described below:

- Inertial reference frame N (X_N, Y_N, Z_N) – This reference frame is selected as the Launch Point Inertial (LPI) frame. The origin is fixed at time $t = 0$ on the Earth's surface directly below the Payload CG. The X_N axis is along the local vertical pointing away from the ground, Z_N lies in the horizontal plane making an angle ψ_L with local north and the Y_N axis completes the right-handed coordinate system.
- B_1 frame (X_{B1}, Y_{B1}, Z_{B1}) – This is the payload body frame with its origin at payload CG O_1. The X_{B1} axis is along the longitudinal axis and positive towards the apex cover, Z_{B1} axis is in the horizontal plane and pointing towards the hatch and the Y_{B1} axis completes the right-handed coordinate system.
- B_2 frame (X_{B2}, Y_{B2}, Z_{B2}) – This is the riser body frame with origin at riser CG O_2 and the X_{B2} axis along the length of the riser pointing towards the parachute confluence point J_2.
- B_3 frame (X_{B3}, Y_{B3}, Z_{B3}) – This is the parachute body frame with its origin at the parachute CG O_3. The X_{B3} axis is along the longitudinal axis of the parachute pointing towards the canopy.

3.3 Vector of generalised coordinates and speeds

The degrees of freedom for this multi-body system are designated as:

- Payload is represented as a rigid body having 6 degrees of freedom – 3 translational degrees of freedom in the inertial space, given by $^N\vec{r}_0 = (x_0, y_0, z_0)$ and 3 rotational degrees of freedom about the CG O_1, denoted by space-fixed Euler angle θ_{pay} and intermediate body-fixed Euler angles ψ_{pay} and ϕ_{pay}. The rotational transformation from the N frame to the B_1 frame is characterised using the following sequence of rotation:

$$N \xrightarrow[\text{by } \theta_{pay}]{\text{about } Y} B_1' \xrightarrow[\text{by } \psi_{pay}]{\text{about } Z} B_1'' \xrightarrow[\text{by } \phi_{pay}]{\text{about } X} B_1.$$

The rotation matrix is derived using the methodology as mentioned in Henderson (1977) [6]:

$$^N C^{B1} = \left(^{B1}C^N\right)^T$$

$$
= \begin{bmatrix}
\cos\theta_{pay}\cos\psi_{pay} & \begin{matrix}-\cos\theta_{pay}\sin\psi_{pay}\cos\phi_{pay}\\ +\sin\theta_{pay}\sin\phi_{pay}\end{matrix} & \begin{matrix}\cos\theta_{pay}\sin\psi_{pay}\sin\phi_{pay}\\ +\sin\theta_{pay}\cos\phi_{pay}\end{matrix} \\
\sin\psi_{pay} & \cos\psi_{pay}\cos\phi_{pay} & -\cos\psi_{pay}\sin\phi_{pay} \\
\begin{matrix}-\sin\theta_{pay}\cos\psi_{pay}\end{matrix} & \begin{matrix}\sin\theta_{pay}\sin\psi_{pay}\cos\phi_{pay}\\ +\cos\theta_{pay}\sin\phi_{pay}\end{matrix} & \begin{matrix}-\sin\theta_{pay}\sin\psi_{pay}\sin\phi_{pay}\\ +\cos\theta_{pay}\cos\phi_{pay}\end{matrix}
\end{bmatrix}.
\tag{4}
$$

– The riser B_2 has 2 rotational degrees of freedom about the joint J_1, denoted by the body-fixed relative Euler angles θ_{riser} and ψ_{riser} and 1 translational degree of freedom due to its elastic property, i.e. L_{riser}. The rotational transformation from the B_1 frame to the B_2 frame is characterised using the following order of rotation:

$$
B_1 \xrightarrow[\text{by } \theta_{riser}]{\text{about } Y} B_2' \xrightarrow[\text{by } \psi_{riser}]{\text{about } Z} B_2.
$$

The rotation matrix corresponding to the rotation sequence is

$$
{}^{B1}C^{B2} = \left({}^{B2}C^{B1}\right)^T = \begin{bmatrix}
\cos\theta_{riser}\cos\psi_{riser} & -\cos\theta_{riser}\sin\psi_{riser} & \sin\theta_{riser} \\
\sin\psi_{riser} & \cos\psi_{riser} & 0 \\
-\sin\theta_{riser}\cos\psi_{riser} & \sin\theta_{riser}\sin\psi_{riser} & \cos\theta_{riser}
\end{bmatrix}.
\tag{5}
$$

– Parachute B_3 is considered a rigid body having 3 rotational degrees of freedom about the joint J_2, denoted by the body-fixed relative Euler angles θ_{par}, ϕ_{par} and ψ_{par}. The following order of rotation defines the rotational transformation from B_2 to B_3 frame:

$$
B_2 \xrightarrow[\text{by } \theta_{par}]{\text{about } Y} B_3' \xrightarrow[\text{by } \phi_{par}]{\text{about } X} B_3'' \xrightarrow[\text{by } \psi_{par}]{\text{about } Z} B_3.
$$

The rotation matrix is given by

$$
{}^{B2}C^{B3} = \left({}^{B3}C^{B2}\right)^T
$$
$$
= \begin{bmatrix}
\begin{matrix}\sin\theta_{par}\sin\phi_{par}\sin\psi_{par}\\ +\cos\theta_{par}\cos\psi_{par}\end{matrix} & \begin{matrix}\sin\theta_{par}\sin\phi_{par}\cos\psi_{par}\\ -\cos\theta_{par}\sin\psi_{par}\end{matrix} & \sin\theta_{par}\cos\phi_{par} \\
\cos\phi_{par}\sin\psi_{par} & \cos\phi_{par}\cos\psi_{par} & -\sin\phi_{par} \\
\begin{matrix}\cos\theta_{par}\sin\phi_{par}\sin\psi_{par}\\ -\sin\theta_{par}\cos\psi_{par}\end{matrix} & \begin{matrix}\cos\theta_{par}\sin\phi_{par}\cos\psi_{par}\\ +\sin\theta_{par}\sin\psi_{par}\end{matrix} & \cos\theta_{par}\cos\phi_{par}
\end{bmatrix}.
\tag{6}
$$

Based on the 12 degrees of freedom of the system, the selected generalised speeds are represented as a column vector as follows:

$$
\vec{u} = [\vec{\omega}_1, \sigma_2, \sigma_3, \vec{v}_1, \dot{L}_{riser}]^T,
\tag{7}
$$

where,

$$
\vec{\omega}_1 = \begin{Bmatrix} p_{pay} \\ q_{pay} \\ r_{pay} \end{Bmatrix}, \quad
\sigma_2 = \begin{Bmatrix} \dot{\theta}_{riser} \\ \dot{\psi}_{riser} \end{Bmatrix}, \quad
\sigma_3 = \begin{Bmatrix} \dot{\theta}_{par} \\ \dot{\phi}_{par} \\ \dot{\psi}_{par} \end{Bmatrix}, \quad
\vec{v}_1 = \begin{Bmatrix} \dot{x}_0 \\ \dot{y}_0 \\ \dot{z}_0 \end{Bmatrix}.
\tag{8}
$$

3.4 Derivation of equations of motion

The relative angular body rates of each of the bodies (ω) can be represented in terms of the joint angular rates (σ) using a *"joint partial matrix (Γ) [16]"* as follows:

$$^{B1}\vec{\omega}^{B1/N} = \vec{\omega}_1, \qquad ^{B2}\vec{\omega}^{B2/B1} = \Gamma_2\sigma_2, \qquad ^{B3}\vec{\omega}^{B3/B2} = \Gamma_3\sigma_3, \tag{9}$$

where,

$$\Gamma_2 = \begin{bmatrix} \sin\psi_{riser} & 0 \\ \cos\psi_{riser} & 0 \\ 0 & 1 \end{bmatrix}, \Gamma_3 = \begin{bmatrix} \cos\phi_{par}\sin\psi_{par} & \cos\psi_{par} & 0 \\ \cos\phi_{par}\cos\psi_{par} & -\sin\psi_{par} & 0 \\ -\sin\phi_{par} & 0 & 1 \end{bmatrix}. \tag{10}$$

The angular velocities of the three bodies B_i, $i = 1, 2, 3$, with respect to the inertial frame N expressed in the corresponding body frame can be derived as:

$$^{B1}\vec{\omega}^{B1/N} = \vec{\omega}_1, \tag{11a}$$

$$^{B2}\vec{\omega}^{B2/N} = {}^{B2}C^{B1B1}\vec{\omega}^{B1/N} + {}^{B2}\vec{\omega}^{B2/B1}$$
$$= {}^{B2}C^{B1}\omega_1 + \Gamma_2\sigma_2, \tag{11b}$$

$$^{B3}\vec{\omega}^{B3/N} = {}^{B3}C^{B2B2}\vec{\omega}^{B2/N} + {}^{B3}\vec{\omega}^{B3/B2}$$
$$= {}^{B3}C^{B1}\omega_1 + {}^{B3}C^{B2}\Gamma_2\sigma_2 + \Gamma_3\sigma_3. \tag{11c}$$

Angular velocities derived in Equation (11a)–(11c) can be added together to form the *"partial angular velocity matrix (Ω) [16]"*, consisting of partial derivatives of angular velocity with respect to the generalised speeds of the system:

$$\begin{bmatrix} ^{B1}\vec{\omega}^{B1/N} \\ ^{B2}\vec{\omega}^{B2/N} \\ ^{B3}\vec{\omega}^{B3/N} \end{bmatrix} = \underbrace{\begin{bmatrix} I_{3\times3} & 0_{3\times2} & 0_{3\times3} & 0_{3\times3} & 0_{3\times1} \\ ^{B2}C^{B1} & \Gamma_2 & 0_{3\times3} & 0_{3\times3} & 0_{3\times1} \\ ^{B3}C^{B1} & ^{B3}C^{B2}\Gamma_2 & \Gamma_3 & 0_{3\times3} & 0_{3\times1} \end{bmatrix}}_{\Omega} \vec{u}. \tag{12}$$

Subsequently, the angular acceleration of the each of the bodies B_i, $i = 1, 2, 3$ with respect to frame N expressed in their corresponding body frame can be derived, as mentioned in Pal (2020) [12]:

$$^{B1}\vec{\alpha}^{B1/N} = {}^{B1}\dot{\vec{\omega}}^{B1/N}, \tag{13a}$$

$$^{B2}\vec{\alpha}^{B2/N} = {}^{B2}C^{B1B1}\dot{\vec{\omega}}^{B1/N} + \Gamma_2\dot{\sigma}_2 + {}^{B2}\vec{\alpha}_r^{B2/N}, \tag{13b}$$

$$^{B3}\vec{\alpha}^{B3/N} = {}^{B3}C^{B1B1}\dot{\vec{\omega}}^{B1/N} + {}^{B3}C^{B2}\Gamma_2\dot{\sigma}_2 + \Gamma_3\dot{\sigma}_3 + {}^{B3}\vec{\alpha}_r^{B3/N}, \tag{13c}$$

where $^{B2}\vec{\alpha}_r^{B2/N}$ and $^{B3}\vec{\alpha}_r^{B3/N}$ are the *"remainder angular accelerations [16]"*, and $\dot{\Gamma}_2$ and $\dot{\Gamma}_3$ are the time derivatives of the joint partial matrices Γ_2 and Γ_3, respectively:

$$^{B2}\vec{\alpha}_r^{B2/N} = \dot{\Gamma}_2\sigma_2 + \left({}^{B2}C^{B1}\,\vec{\omega}_1\right) \times {}^{B2}\vec{\omega}^{B2/B1}, \tag{14a}$$

$$\dot{\Gamma}_2 = \begin{bmatrix} \dot{\psi}_{riser}\cos\psi_{riser} & 0 \\ -\dot{\psi}_{riser}\sin\psi_{riser} & 0 \\ 0 & 0 \end{bmatrix}, \tag{14b}$$

$$^{B3}\vec{\alpha}_r^{B3/N} = {}^{B3}\vec{\alpha}_r^{B2/N} + \dot{\Gamma}_3\sigma_3 + \left({}^{B3}\vec{\omega}^{B2/N}\right) \times {}^{B3}\vec{\omega}^{B3/B2}, \tag{14c}$$

$$\dot{\Gamma}_3 = \begin{bmatrix} -\dot{\phi}_{par}\sin\phi_{par}\sin\psi_{par} + \dot{\psi}_{par}\cos\phi_{par}\cos\psi_{par} & -\dot{\psi}_{par}\sin\psi_{par} & 0 \\ -\dot{\phi}_{par}\sin\phi_{par}\cos\psi_{par} - \dot{\psi}_{par}\cos\phi_{par}\sin\psi_{par} & -\dot{\psi}_{par}\cos\psi_{par} & 0 \\ -\dot{\phi}_{par}\cos\phi_{par} & 0 & 0 \end{bmatrix}. \tag{14d}$$

Next, the position of the CGs of the three bodies O_i, $i = 1, 2, 3$ as well as the joints J_i, $i = 1, 2$ are derived with respect to a point n fixed in the inertial space (assumed to be the CG of the inertial frame N) and expressed in the inertial frame N:

$$^{N}\vec{r}^{O_1/O_N} = {}^{N}\vec{r}_0, \tag{15a}$$

$$^{N}\vec{r}^{J_1/O_N} = {}^{N}\vec{r}^{O_1/O_N} + {}^{N}C^{B1B1}\vec{r}^{J_1/O_1}, \tag{15b}$$

$$^{N}\vec{r}^{O_2/O_N} = {}^{N}\vec{r}^{J_1/O_N} - {}^{N}C^{B2B2}\vec{r}^{J_1/O_2}, \tag{15c}$$

$$^{N}\vec{r}^{J_2/O_N} = {}^{N}\vec{r}^{O_2/O_N} + {}^{N}C^{B2B2}\vec{r}^{J_2/O_2}, \tag{15d}$$

$$^{N}\vec{r}^{O_3/O_N} = {}^{N}\vec{r}^{J_2/O_N} - {}^{N}C^{B3B3}\vec{r}^{J_2/O_3}, \tag{15e}$$

where,

- $^{B1}\vec{r}^{J_1/O_1}$ is derived based on the riser attachment point on the payload.
- $^{B2}\vec{r}^{J_1/O_2}$ and $^{B2}\vec{r}^{J_2/O_2}$ satisfy the following equation assuming that the riser has a uniform mass distribution

$$\begin{bmatrix} \frac{L_{riser}}{2} \\ 0 \\ 0 \end{bmatrix} = -{}^{B2}\vec{r}^{J_1/O_2} = {}^{B2}\vec{r}^{J_2/O_2}. \tag{16}$$

- $^{B3}\vec{r}^{J_2/O_3}$ is worked out based on the Parachute centre of mass, which has been derived as per Ibrahim and Engdahl (1974) [8] assuming the parachute canopy is a semi-oblate spheroid with instantaneous height h, radius r and mass m_C, and suspension lines having length L_s and mass m_L:

$$^{B3}\vec{r}^{J_2/O_3} = \begin{bmatrix} -L_{cm} \\ 0 \\ 0 \end{bmatrix} = \begin{bmatrix} -\frac{(m_L L_{cms}) + (m_C L_1) + (m_I L_1)}{m_L + m_C + m_I} \\ 0 \\ 0 \end{bmatrix}, \tag{17}$$

where, L_{cm} is the centre of mass of the parachute, which is derived considering the included mass of the canopy $m_I = \frac{2}{3}\rho\pi r^2 h$, the density of the atmosphere ρ, the centre of mass of the canopy and the included mass L_1 and the centre of mass of the suspension lines of the parachute L_{cms}.

$$L_{cms} = (0.5 L_s \cos(\sin^{-1}(\frac{r}{L_s}))). \tag{18}$$

The instantaneous height h and radius r are computed by multiplying the steady-state canopy radius and height as derived in Ibrahim and Engdahl (1974) [8] with f_{inf} as derived in Equation (33).

Now, the velocity of the CGs for each of the bodies with respect to the inertial frame origin expressed in the inertial frame N can be computed as in Equation (19a)–(19c):

$$^{N}\vec{v}^{O_1/O_N} = \vec{v}_1, \tag{19a}$$

$$
{}^N\vec{v}^{O_2/O_N} = {}^N\vec{v}^{O_1/O_N} + \left({}^N\vec{r}^{O_1/O_2} \times {}^N C^{B1B1}\vec{\omega}^{B1/N}\right)
$$

$$
+ \left({}^N\vec{r}^{J_1/O_2} \times {}^N C^{B2B2}\vec{\omega}^{B2/B1}\right) \tag{19b}
$$

$$
+ {}^N C^{B2}\frac{\dot{L}_{riser}}{2},
$$

$$
{}^N\vec{v}^{O_3/O_N} = {}^N\vec{v}^{O_1/O_N} + \left({}^N\vec{r}^{O_1/O_3} \times {}^N C^{B1B1}\vec{\omega}^{B1/N}\right)
$$

$$
+ \left({}^N\vec{r}^{J_1/O_3} \times {}^N C^{B2B2}\vec{\omega}^{B2/B1}\right) + \left({}^N\vec{r}^{J_2/O_3} \times {}^N C^{B3B3}\vec{\omega}^{B3/B2}\right) \tag{19c}
$$

$$
+ {}^N C^{B2}\dot{L}_{riser}.
$$

The angular velocities of the bodies can be expanded in terms of generalised speeds as mentioned in Equation (11a)–(11c) and then, Equation (19a)–(19c) can be grouped to form the *"partial velocity matrix V [16]"*, derived in Equation (20):

$$
\begin{bmatrix} {}^N\vec{v}^{O_1/O_N} \\ {}^N\vec{v}^{O_2/O_N} \\ {}^N\vec{v}^{O_3/O_N} \end{bmatrix} = \underbrace{\begin{bmatrix} 0_{3\times3} & 0_{3\times2} & 0_{3\times3} & I_{3\times3} & 0_{3\times1} \\ {}^N r_\times^{O_1/O_2}{}^N C^{B1} & {}^N r_\times^{J_1/O_2}{}^N C^{B2}\Gamma_2 & 0_{3\times3} & I_{3\times3} & {}^N C^{B2}/2 \\ {}^N r_\times^{O_1/O_3}{}^N C^{B1} & {}^N r_\times^{J_1/O_3}{}^N C^{B2}\Gamma_2 & {}^N r_\times^{J_2/O_3}{}^N C^{B3}\Gamma_3 & I_{3\times3} & {}^N C^{B2} \end{bmatrix}}_{V}\vec{u}.
$$

$$\tag{20}$$

${}^N r_\times^{J_1/O_2}$ and other similar terms in Equation (20) are skew-symmetric matrices of vectors, which equivalently perform a cross-product of the given vector with some other vector.

Next, the accelerations of the points O_1, O_2 and O_3, with respect to the origin of the inertial frame are expressed as

$$
{}^N\vec{a}^{O_1/O_N} = {}^N\dot{\vec{v}}_1, \tag{21a}
$$

$$
{}^N\vec{a}^{O_2/O_N} = {}^N\vec{a}^{O_1/O_N}
$$

$$
+ {}^N C^{B1B1}\dot{\vec{\omega}}^{B1/N} \times {}^N\vec{r}^{O_2/O_1} + {}^N C^{B2}\Gamma_2\dot{\sigma}_2 \times {}^N\vec{r}^{O_2/J_1} \tag{21b}
$$

$$
+ {}^N\vec{\omega}^{B2/N} \times {}^N C^{B2}\dot{L}_{riser} + {}^N\vec{a}_r^{O_2/n},
$$

$$
{}^N\vec{a}^{O_3/O_N} = {}^N\vec{a}^{O_1/O_N}
$$

$$
+ {}^N C^{B1B1}\dot{\vec{\omega}}^{B1/N} \times {}^N\vec{r}^{O_3/O_1} + {}^N C^{B2}\Gamma_2\dot{\sigma}_2 \times {}^N\vec{r}^{O_3/J_1} \tag{21c}
$$

$$
+ {}^N C^{B3}\Gamma_3\dot{\sigma}_3 \times {}^N\vec{r}^{O_3/J_2} + 2 \times {}^N\vec{\omega}^{B2/N} \times {}^N C^{B2}\dot{L}_{riser} + {}^N\vec{a}_r^{O_3/n},
$$

where the *"remainder accelerations [16]"* ${}^N\vec{a}_r^{O_2/O_N}$ and ${}^N\vec{a}_r^{O_3/O_N}$ are

$$
{}^N\vec{a}_r^{O_2/O_N} = {}^N C^{B2B2}\vec{\alpha}_r^{B2/N} \times {}^N\vec{r}^{O_2/J_1}
$$

$$
+ {}^N\vec{\omega}^{B1/N} \times \left({}^N\vec{\omega}^{B1/N} \times {}^N\vec{r}^{J_1/O_1}\right) + {}^N\vec{\omega}^{B2/N} \times \left({}^N\vec{\omega}^{B2/N} \times {}^N\vec{r}^{O_2/J_1}\right), \tag{22a}
$$

$$
{}^N\vec{a}_r^{O_3/O_N} = {}^N\vec{a}_r^{O_2/O_N}
$$

$$
+ {}^N C^{B2B2}\vec{\alpha}_r^{B2/N} \times {}^N\vec{r}^{J_2/O_2} + {}^N C^{B3B3}\vec{\alpha}_r^{B3/N} \times {}^N\vec{r}^{O_3/J_2} \tag{22b}
$$

$$
+ {}^N\vec{\omega}^{B2/N} \times \left({}^N\vec{\omega}^{B2/N} \times {}^N\vec{r}^{J_2/O_2}\right) + {}^N\vec{\omega}^{B3/N} \times \left({}^N\vec{\omega}^{B3/N} \times {}^N\vec{r}^{O_3/J_2}\right),
$$

$$
{}^N\vec{\omega}^{B1/N} = {}^N C^{B1}\,{}^{B1}\vec{\omega}^{B1/N}, \qquad {}^N\vec{\omega}^{B2/N} = {}^N C^{B2}\,{}^{B2}\vec{\omega}^{B2/N}, \qquad {}^N\vec{\omega}^{B3/N} = {}^N C^{B3}\,{}^{B3}\vec{\omega}^{B3/N}.
$$

$$\tag{22c}$$

The active forces and moments acting on the system are the force due to gravity, aerodynamic forces and moments, and forces and moments due to elasticity of the riser. Furthermore, during the parachute deployment and inflation phase, an additional generalised thrust is also added to cater for the effects due to variable mass, as described in Ge et al. (1982) [3].

The translational kinematics of the systems are derived in an inertial frame as seen from Equations (15a)–(15e), (19a)–(19c) and (21a)–(21c), hence the active forces are to be expressed in the inertial frame, with translational dynamics being solved in the inertial frame. Similarly, inspection of Equations (11a)–(11c) and (13a)–(13c), clearly shows that rotational dynamics is to be solved in the body frame requiring the active moments to be expressed in the corresponding body frame.

For body B_1, i.e. payload, the active forces and moments acting are

$$^N \vec{F}^{B_1} = {}^N \vec{F}_G^{B_1} + {}^N \vec{F}_A^{B_1} + {}^N \vec{F}_S^{B_1} + {}^N \vec{F}_{ME}^{B_1}, \tag{23a}$$

$$^{B1} \vec{M}^{B_1/O_1} = {}^{B1} \vec{M}_A^{B_1/O_1} + {}^{B1} \vec{M}_S^{B_1/O_1} + {}^{B1} \vec{M}_{ME}^{B_1/O_1}. \tag{23b}$$

For body B_2, i.e. the riser, the active forces and moments acting are

$$^N \vec{F}^{B_2} = {}^N \vec{F}_G^{B_2}, \tag{24a}$$

$$^{B2} \vec{M}^{B_2/O_2} = 0_{3\times 1} \tag{24b}$$

and for body B_3, i.e. the parachute, they are

$$^N \vec{F}^{B_3} = {}^N \vec{F}_G^{B_3} + {}^N \vec{F}_A^{B_3} + {}^N \vec{F}_S^{B_3} + {}^N \vec{F}_{GT}^{B_3}, \tag{25a}$$

$$^{B3} \vec{M}^{B_3/O_3} = {}^{B3} \vec{M}_A^{B_3/O_3} + {}^{B3} \vec{M}_S^{B_3/O_3}, \tag{25b}$$

where, $\vec{F}_G$, $\vec{F}_A$, $\vec{F}_S$ and $\vec{F}_{ME}$ are the gravitational force, aerodynamic force, elastic spring force, and mass ejection force, respectively, and $\vec{M}_A$, $\vec{M}_S$ and $\vec{M}_{ME}$ are the aerodynamic moment, spring moment and mass ejection moment, respectively.

Considering the flat-Earth assumption, the gravitational forces acting on all the three bodies expressed in the inertial frame N can be written as

$$^N \vec{F}_G^{B_i} = \begin{Bmatrix} -m_i g \\ 0 \\ 0 \end{Bmatrix}, \tag{26}$$

where, m_i is the mass of body B_i, $i = 1, 2, 3$, and g is the acceleration due to gravity.

The spring force caused by elasticity of the riser is computed in the riser body frame B_2 as

$$^{B2} \vec{F}_S^{B_3} = -{}^{B2} \vec{F}_S^{B_1} = \begin{Bmatrix} K(\Delta L_{riser}) - \zeta \dot{L}_{riser} \\ 0 \\ 0 \end{Bmatrix}, \tag{27}$$

where, K and ζ are the spring constant and damping constant for the elastic riser.

$\vec{F}_{GT}$ is the generalised thrust added to the parachute to cater for the variable-mass effects during the deployment and inflation phase as described in Ke et al. (2009) [10], with the

equation

$$
{}^{B3}\vec{F}_{GT}^{B3} = \begin{Bmatrix} \dot{m}\dot{l} \\ 0 \\ 0 \end{Bmatrix}.
\tag{28}
$$

The mass ejection force and moment acting on the payload CG expressed in its body frame is derived as follows:

$$
{}^{B1}\vec{F}_{ME}^{B1} = \dot{m}\left({}^{B1}\omega^{B1/N} \times {}^{B1}r^{J_1/O_1}\right), \quad {}^{B1}\vec{M}_{ME}^{B1/O_1} = {}^{B1}r^{J_1/O_1} \times {}^{B1}\vec{F}_{ME}^{B1}.
\tag{29}
$$

The aerodynamic forces and moments acting on the payload and the parachute CGs ($i = 1, 3$) are expressed in their corresponding body frames as:

$$
{}^{Bi}\vec{F}_A^{Bi} = f_{inf} \begin{Bmatrix} C_{A,i}\,Q_i\,S_i \\ C_{S,i}\,Q_i\,S_i \\ C_{N,i}\,Q_i\,S_i \end{Bmatrix}, \quad {}^{Bi}\vec{M}_A^{Bi/O_i} = f_{inf} \begin{Bmatrix} C_{RM,i}\,Q_i\,S_i\,L_i \\ C_{PM,i}\,Q_i\,S_i\,L_i \\ C_{YM,i}\,Q_i\,S_i\,L_i \end{Bmatrix} + {}^{Bi}r^{O_i/CP_i} \times {}^{Bi}\vec{F}_A^{Bi},
\tag{30}
$$

where S_i is the reference area, L_i is the reference length and Q_i is the dynamic pressure of the ith body. Since, the payload acts as a forebody to the parachute, Q_{par} would not be the freestream dynamic pressure. Hence, a simplistic model as given in Peterson and Johnson (2013) [15] is incorporated to simulate the wake effects, which consists of empirical constants (a,k,m and n) proposed by Heinrich and Eckstrom (1963) [5]:

$$
Q_{par} = Q_\infty \times \left(1 + \left(\frac{2}{r^2}\frac{D_1}{D_2}\left[1 - e^{D_2 r^2} + \frac{D_1}{4}e^{2D_2 r^2} - \frac{D_1}{4}\right]\right)\right),
\tag{31}
$$

where,

$$
D_1 = \frac{a}{(Z/D_B)^m} \qquad \text{and} \qquad D_2 = \frac{-1}{0.435 k^2 (Z/D_B)^{2n}}.
\tag{32}
$$

f_{inf} is the inflation factor that models the increase in drag and normal forces during the parachute-inflation phase. The force factor is modelled as shown in Equation (33) with the interpolation scheme considered to be linear interpolation and f_{reef} being the ratio of reefing of the canopy:

$$
f_{inf} = \begin{cases} 0 & \text{for } t < t_{stretch}, \\ \text{interpolation }(t, [0,\ f_{reef}]) & \text{for } t_{stretch} \leq t < t_{stretch} + t_{inflate}, \\ f_{reef} & \text{for } t_{stretch} + t_{inflate} \leq t < t_{stretch} + t_{reef\ cut}, \\ \text{interpolation }(t, [f_{reef},\ 1]) & \text{for } t_{stretch} + t_{reef\ cut} \leq t \\ & \quad < t_{stretch} + t_{reef\ cut} + t_{disreef}, \\ 1 & \text{for } t \geq t_{stretch} + t_{reef\ cut} + t_{disreef}. \end{cases}
\tag{33}
$$

The remaining terms in Equation (3), i.e [m], [I], $\{\omega\}$, $\{\alpha_r\}$, $\{a_r\}$, $\{F\}$ and $\{M\}$ are derived as follows:

$$
[m] = \begin{bmatrix} m_1 I_{3\times 3} & 0 & 0 \\ 0 & m_2 I_{3\times 3} & 0 \\ 0 & 0 & (m_3 + m_{3A})I_{3\times 3} \end{bmatrix}, \quad [I] = \begin{bmatrix} I^{B_1/O_1} & 0 & 0 \\ 0 & I^{B_2/O_2} & 0 \\ 0 & 0 & I^{B_3/O_3} \end{bmatrix},
\tag{34a}
$$

$$\{\omega\} = \begin{Bmatrix} B1\vec{\omega}^{B1/N} \\ B2\vec{\omega}^{B2/N} \\ B3\vec{\omega}^{B3/N} \end{Bmatrix}, \quad \{\alpha_r\} = \begin{Bmatrix} B1\vec{\alpha}_r^{B1/N} \\ B2\vec{\alpha}_r^{B2/N} \\ B3\vec{\alpha}_r^{B3/N} \end{Bmatrix}, \quad \{a_r\} = \begin{Bmatrix} N\vec{a}_r^{O1/O_N} \\ N\vec{a}_r^{O2/O_N} \\ N\vec{a}_r^{O3/O_N} \end{Bmatrix}, \tag{34b}$$

$$\{F\} = \begin{Bmatrix} N\vec{F}^{B_1} \\ N\vec{F}^{B_2} \\ N\vec{F}^{B_3} \end{Bmatrix}, \quad \{M\} = \begin{Bmatrix} B1\vec{M}^{B_1/O_1} \\ B2\vec{M}^{B_2/O_2} \\ B3\vec{M}^{B_3/O_3} \end{Bmatrix}, \tag{34c}$$

where, I^{B_1/O_1}, I^{B_2/O_2} and I^{B_3/O_3} are the inertia matrices of the bodies B_1, B_2 and B_3, respectively, and m_{3A} is the apparent mass of the parachute.

– m_{3A} is computed considering the potential flow around the semi-oblate spheroid geometry of the canopy as described in Kidane (2009) [11]:

$$m_{3A} = \frac{\alpha_0}{2 - \alpha_0} \frac{2}{3} \rho \pi r^2 h, \tag{35a}$$

$$\alpha_0 = r^2 h \int_0^\infty \frac{d\lambda}{(h^2 + \lambda)(r^2 + \lambda)\sqrt{(h^2 + \lambda)}}. \tag{35b}$$

– I^{B_1/O_1} is the inertia tensor of the payload, which is an input.
– I^{B_2/O_2} can be computed assuming the riser to be a uniform cylindrical rod of infinitesimally small radius, which would result in

$$I^{B_2/O_2} = \begin{bmatrix} 0 & 0 & 0 \\ 0 & \frac{m_2 L_{riser}^2}{12} & 0 \\ 0 & 0 & \frac{m_2 L_{riser}^2}{12} \end{bmatrix}. \tag{36}$$

– The inertia tensor for the parachute, i.e. I^{B_3/O_3} is derived as expressed in Ibrahim and Engdahl (1974) [8]:

$$I^{B_3/O_3} = \begin{bmatrix} I_{xx} & 0 & 0 \\ 0 & I_{yy} & 0 \\ 0 & 0 & I_{zz} \end{bmatrix}, \tag{37}$$

where,

$$I_{xx} = \frac{1}{12} m_L L_s^2 \sin^2(\sin^{-1}(\frac{r}{L_s})) + \frac{2}{3} m_C r^2 + 0.063 \rho R_0^5, \tag{38a}$$

$$I_{zz} = I_{yy} = \frac{1}{12} m_L L_s^2 \cos^2(\sin^{-1}(\frac{r}{L_s})) + m_L (L_{cms} - L_{cm})^2$$
$$+ \frac{1}{3} m_C (h^2 + r^2) + m_{3A} (L_1 - L_{cm})^2 \tag{38b}$$
$$+ m_{3A} (L_1 - L_{cm})^2 + 0.042 \rho R_0^5.$$

All the above terms are assembled into Equation (3), to form the system of equations describing the dynamics of the Parachute–Elastic Riser–Payload System.

Table 2 Model parameters used in validation simulation

Parameters	Value
g	9.80665 m·s^{-2}
m_1	69,321 kg
m_2	1×10^{-6} kg
m_3	2210.991 kg
m_C	1020.121 kg
m_L	1190.87 kg
$I_{xx}^{B_1/O_1}$	2,259,151 kg·m^2
$I_{yy}^{B_1/O_1}$	9,667,065.6 kg·m^2
$I_{zz}^{B_1/O_1}$	9,667,065.6 kg·m^2
$^{B1}\vec{r}^{J_1/O_1}$	(25, 0, 0) m
L_{riser}	20.1 m
L_s	82.5 m
L_1	93 m
R_0	18.5 m
h	12.675 m
r	14.04 m

4 Results and validation

This section describes the simulations carried out using the formulated model and analysis of the results. The matrix form of the equations derived in Equation (3) is solved at each instant using a LU-decomposition solver implemented in C++ to obtain the generalised accelerations $\dot{\vec{u}}$. These are integrated to obtain the generalised speed $\vec{u}$ that involves the attitude and position of the payload and the joint angles for the riser and parachute [12].

The developed model is validated by modelling the SRB parachute-recovery system using Newton–Euler formulation as described in Ibrahim and Engdahl (1974) [8] and subjecting the system to a 20 deg pendulum disturbance at an altitude of 1800 m and initial downward velocity of 60 m/s. Furthermore, the reference literature assumes the riser to be a massless body that transmits only axial forces to the attachment points, which has been modelled by forcing m_{riser} to be an extremely small value. Additionally, the literature also considers the simulation starts at the time instant when the parachute is fully deployed and inflated. The simulation has been carried out assuming a flat-Earth model and altitude-based density variation considering the Indian Standard Atmosphere. Table 2 gives the system parameters used for validation.

The aerodynamic coefficients of SRB and parachute are given in polynomial form described in Equation (39), with the polynomial coefficients as mentioned in Ibrahim and Engadhl (1974) [8] and tabulated in Table 3:

$$C_{A/N/PM} = \sum_{i=0}^{N} p_i * \alpha^i. \tag{39}$$

Figure 2 shows an exact match between the two formulations, validating Kane's formulation for the system.

Furthermore, experiments to quantify the advantage offered by Kane's method over the Newton–Euler method in terms of time complexity is carried out by running 100 simulations with the above model considering varying initial conditions, on a system with an Intel

Table 3 Polynominal Coefficients for Aerodynamics Modelling (Ref: [8])

Coefficients	p_0	p_1	p_2	p_3	p_4
CA_{SRB}	0.6989	$0.1915E^{-8}$	12.56	$-0.1682E^{-7}$	-35.59
CN_{SRB}	$0.2355E^{-9}$	3.645	$-0.8473E^{-8}$	15.20	$0.4432E^{-7}$
CPM_{SRB}	-0.1927	-7.032	-1.114	-12.87	33.24
CA_{PAR}	0.5755	$-0.1637E^{-10}$	-0.8091	$0.3483E^{-10}$	0.4228
CN_{PAR}	$0.2172E^{-11}$	0.3795	$-0.9339E^{-11}$	0.3631	0.0
CPM_{PAR}	$-0.7229E^{-4}$	-0.2742	$0.2576E^{-2}$	-1.271	-0.02333
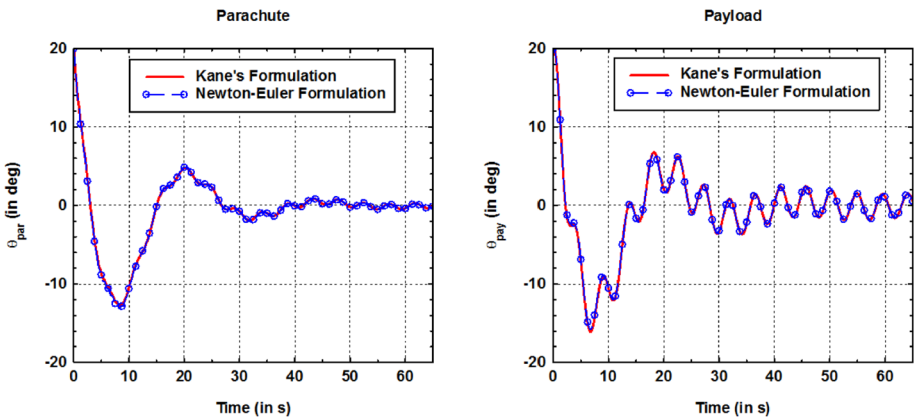
Fig. 2 Pitch Angles of Parachute and Payload (SRB) w.r.t Inertial Frame

Table 4 Execution time comparison between Kane's method and the Newton–Euler method

Method	Average simulation execution time (s)	Average execution time per integration step (ms)	Average time to solve EoM alone per integration step (ms)
Newton–Euler	1.49	0.149	0.098
Kane	1.33	0.133	0.087
Improvement (%)		10.73	11.23

Core i7-7700 processor, 3.60 GHz clock frequency and 8 GB RAM. Computational gain was quantified by computing the average execution time for each simulation run as well as execution time required for solving the equations of motion (EoM) alone in every integration step. The results from the experiment are given in Table 4 wherein an improvement in average execution time to solve EoM by 11.23% is observed due to the elimination of constraint-force computation and an improvement in execution time per integration step by 10.73% is observed. This advantage is also aided by the modular matrix formulation adopted in this paper.

Next, the correctness of Equation (33) modelling the variation in aerodynamic force during the opening transient is validated by matching the descent velocity in the simulation with the velocity observed in the airdrop tests carried out. The results are shown in Fig. 3, where

Fig. 3 Reconstruction of payload descent velocity during the parachute-opening transients
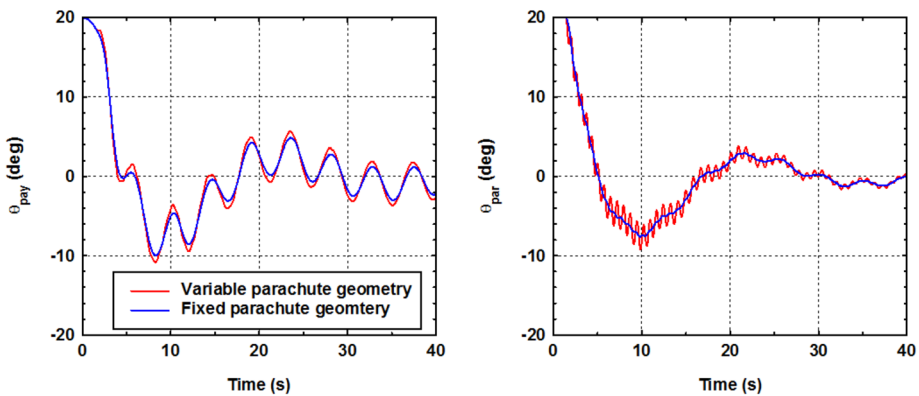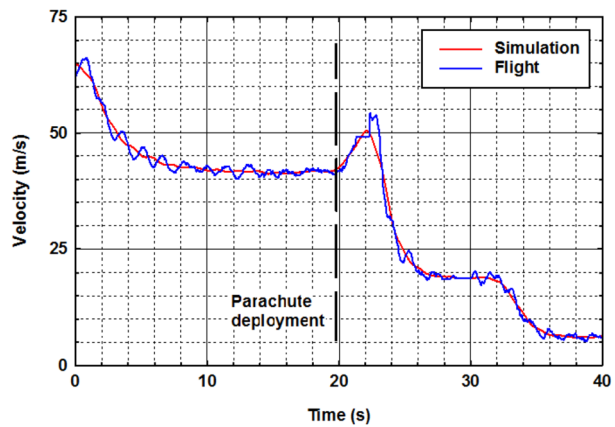

Fig. 4 Effect of variable parachute geometry on the parachute and payload pitch angles

the mean descent velocity is closely captured in the simulation. Oscillations are observed in flight, due to porosity and flexibility of the canopy material (whereas our simulation considers a rigid canopy), which affects the drag of the system. Pei et al. (2019) [14] modelled the canopy breathing, wherein the deformation of the canopy is modelled as a second-order system with an incremental drag modelled as a function of deformation. This incremental drag is added to the basic drag to capture the oscillatory characteristics of the payload velocity.

The variation in attitude of parachute and payload, due to inclusion of varying parachute geometry during the inflation phase, is studied considering a planar simulation with the results shown in Fig. 4. When the parachute geometry is considered fixed, the CG of the parachute L_{cm} is fixed due to a constant included mass m_I of the canopy. When a variable geometry is considered, the mass of included air changes during inflation, and based on Equation (17) the CG of the parachute O_3 is affected. With L_1 assumed to be the centre of pressure (CP) of the parachute, $L_1 - L_{cm}$ (i.e. the distance between CP and CG) defines the stability characteristics of the parachute. In Fig. 5, due to the variable geometry considered, the distance between the parachute CP and CG is higher during the reefed motion, resulting in generation of a higher stabilising moment, and with the absence of damping derivatives in the simulation, higher oscillations in parachute-pitch angles observed in Fig. 4. These higher oscillations affect the total angle of attack of the parachute, affecting the moment exerted by

Fig. 5 Effect of variable parachute geometry on the $CP - CG$ of the parachute
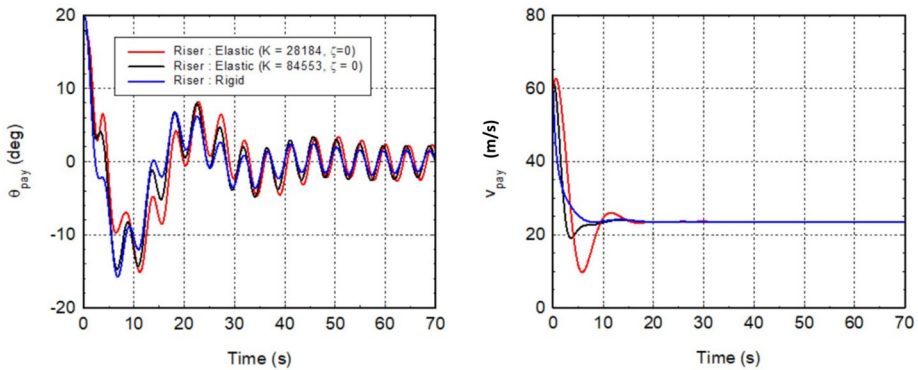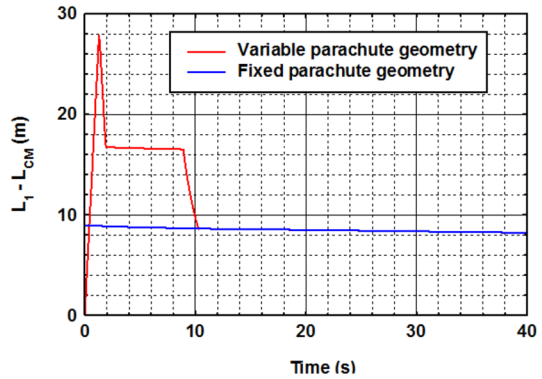

Fig. 6 Effect of riser elasticity on payload velocity and attitude

the parachute on the payload, causing the slightly higher amplitude of oscillations observed in the payload.

The PRPS model formulated in Sect. 3, considers the riser to be an elastic element with the spring force and moment modelled as per Equation (27). The effect of riser flexibility on the trajectory as well as attitude of the payload is shown in Fig. 6. When the riser is modelled as an elastic element, the riser initially elongates as parachute drag acts on one end of the riser and payload gravity acts on the other end, imparting forces in opposite directions. As the elasticity of the riser increases (i.e. the spring constant decreases), the elongation length increases, as seen from Fig. 7. During this elongation, the drag force generated by the parachute is not entirely transferred to the payload, due to which the initial reduction in payload velocity for the elastic model is less than the rigid-body model. Once the riser is elongated enough, a restoring force is generated, which acts on the payload and the parachute. This restoring force acts in the upward direction for the payload, due to which the payload velocity in the downward direction is observed to decrease. It also generates a moment on the payload, which results in the higher variation in amplitude of oscillations in the pitch angle compared to the rigid-body model. The steady-state riser length is determined by the elasticity of the riser, and the amplitude of the pendulum oscillation is observed to be directly proportional to the length of the riser, an observation consistent with the pendulum motion amplitude derived in Pei et al. (2019) [14].

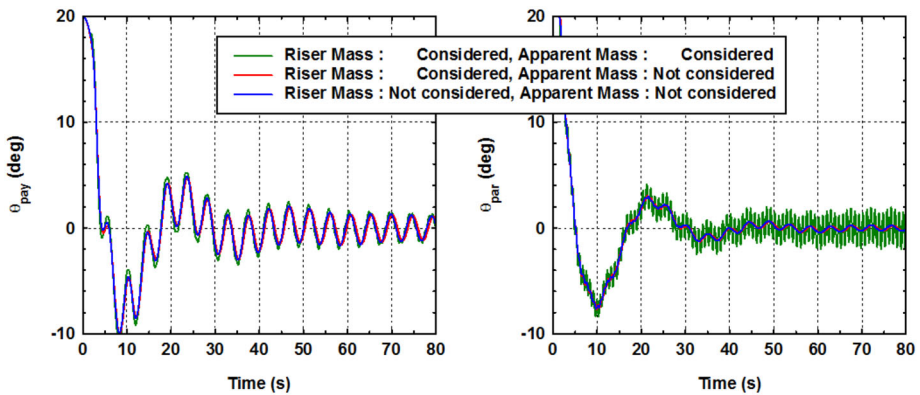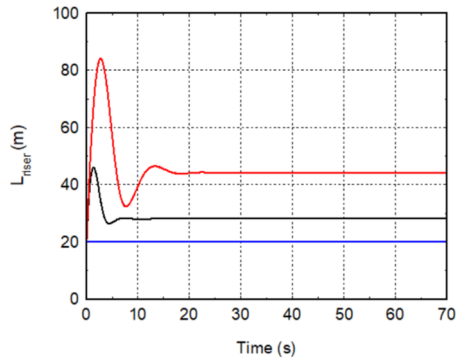**Fig. 7** Effect of riser elasticity on riser elongation

**Fig. 8** Effect of riser mass and parachute apparent mass on parachute and payload pitch angles

The effect of inclusion of the apparent mass (as mentioned in Equation (35b)) and inclusion of the riser mass ($m_2 = 14.594$ kg) is shown in Fig. 8. The effect of riser mass on the system attitude is minimal with the small variation occurring due to the inertia of the riser, which is much small than the inertia of the payload as well as the parachute. Inclusion of the apparent mass on the other hand has comparatively greater effects on the parachute and payload attitude. This is because during the steady-state phase the apparent mass $m_{3A} = 3455.154$ kg is higher than the mass of the canopy $m_3 = 2210.991$ kg itself, which is used in the multi-body mass matrix. Kidane (2009) [11] reported that the effect of apparent mass on parachute drag is minimal, which was also observed from simulations carried out with the model formulated in this paper.

Finally, end-to-end simulations from parachute deployment to separation are carried out by modelling the parachute-opening force in reefed and disreefed modes (as defined in Equation (33)), considering the effects of mass variations and the effect of parachute CG variation during the opening transients. The additional parameters used for this simulation are shown in Table 5.

Figure 9 shows the velocity profile and aerodynamic load profile for an end-to-end parachute simulation. When the time is less than $t_{stretch}$, i.e. when the parachute and riser stretches out of the payload, the aerodynamic load acting on the payload is 0 and the payload velocity increases due to gravity. Once inflation begins, the velocity reduces, which is attributable to increasing parachute drag, and the aerodynamic load first increases as a result

Table 5 Additional parameters used in end-to-end simulations

Parameters	Value
$B1 \vec{r} J_1/O_1$	$(25, 1, 0)$ m
m_2	14.594 kg
$t_{stretch}$	1.28 s
$t_{inflation}$	0.63 s
$t_{reef\ cut}$	7.0 s
$t_{disreef}$	1.4 s
f_{reef}	0.45
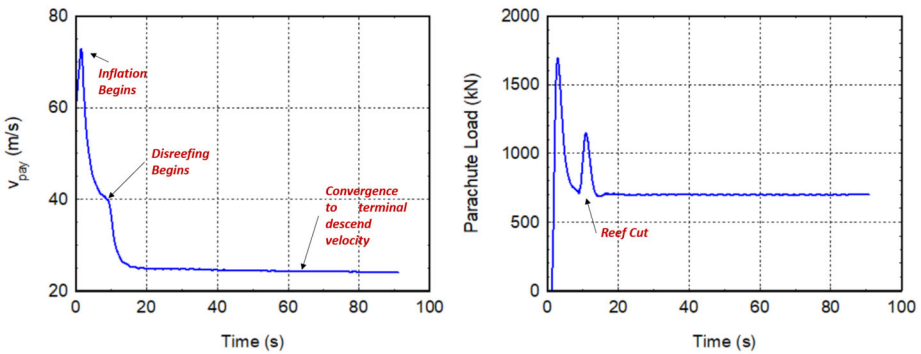
Fig. 9 End-to-end velocity and aerodynamic load profile

of increasing drag of the inflating parachute, followed by an exponential reduction owing to the reduction in dynamic pressure (reducing velocity). A similar profile is observed when disreefing begins. After disreefing, the velocity profile slowly converges to the terminal velocity of descent, but since the simulation considers altitude-based density variation, the velocity tends to convergence only.

The motion of the CGs of the parachute and payload is shown in Fig. 10. During the parachute-deployment phase, the payload descents vertically because of gravity and the parachute CG moves in the lateral direction owing to the stretching of bridles and suspension lines. When inflation begins, the drag builds up, and stable aerodynamic behaviour ensures the initial lateral movement is corrected by the parachute. Post the deployment process, the descent trajectory of the payload is determined by the parachute, where the lateral movement is dependent on the direction of the wind, as the parachute drag force acts opposite to the air relative velocity vector. In the current simulation PRPS movement is predominantly in the eastward direction due to higher zonal wind, as shown in Fig. 11. It is also observed that the pendulum motion undergone by the system is in a plane perpendicular to the dominant motion of the PRPS system.

The rotational states of the system from parachute deployment to splashdown are shown in Fig. 12. The oscillations in inertial pitch and yaw angles define the pendulum motion wherein the parachute and payload oscillate about the mean vertical axis of the inertial frame N. Oscillations in the payload are observed to have higher amplitude because of the pivot point of the pendulum oscillation being closer to the parachute. The inertial yaw angle of the payload, has a steady-state offset from 0° owing to the lateral offset in the attachment point of the riser on the payload, as given in Table 5. The relative joint angles made by the
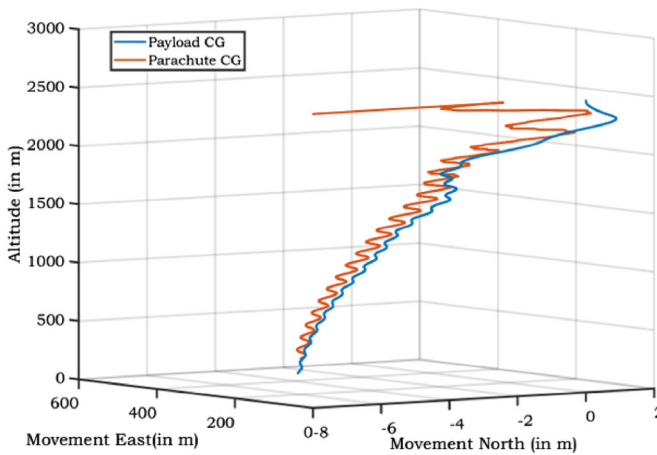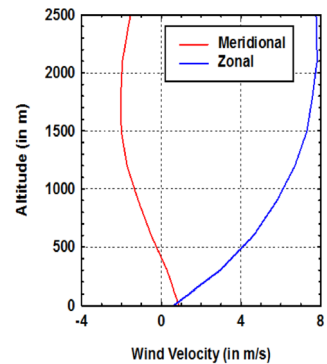
Fig. 10 Trajectories of Payload and Parachute mass centres

Fig. 11 Simulation Wind

riser w.r.t. the payload, and the parachute w.r.t. the riser are plotted in Fig. 12, which clearly indicates that relative motion between parachute and payload predominantly occurs at the riser–payload joint.

5 Conclusion

The dynamics of a Single Parachute–Riser–Payload system, consisting of a Parachute and a Payload sculpted as rigid bodies connected using a elastic riser with non-zero mass, is modelled as a 12-DoF system using the matrix form of Kane's method. A simplistic reaction thrust-based methodology is adopted to model the effects during a parachute-opening transient due to mass ejection.

The formulated model is validated by comparing the achieved results with the results obtained by using Newton–Euler formulation, with an improvement in execution time by 10.73% reported when using the model developed in this paper. This paper also described an accurate modelling of drag variation during the parachute-inflation phase that was validated with flight results. Furthermore, the effect of varying parachute geometry, inclusion of riser mass and apparent mass, on payload and parachute rotational states were also critically
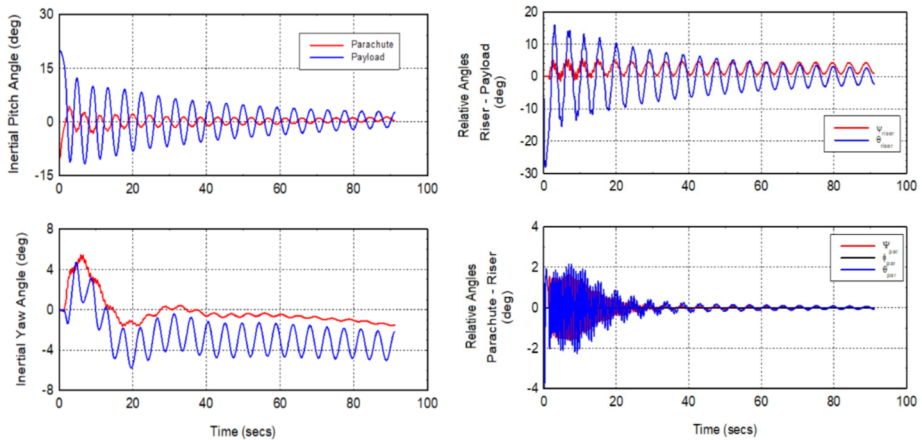
Fig. 12 Inertial and Relative Angles of Parachute and Payload w.r.t. Inertial Frame (End-to-End Simulation)

analysed, with apparent mass and variable parachute geometry observed to have significant effects on the parachute and payload rotational dynamics. The attitude dynamics variation due to modelling the riser as an elastic element is also discussed, with a clear requirement of modelling the riser as an elastic body brought out to simulate the parachute dynamics during the inflation phase with highest accuracy.

The modular matrix formulation of PRPS system ensures that the model can easily be extended to a cluster of parachutes, either by considering a single parachute equivalent to a cluster (using a cluster coefficient factor to be used in parachute aerodynamics) or by extending the derived velocity, mass-inertia and force matrices for multiple parachutes (considering each parachute as separate bodies and modelling the contact aerodynamics). The fidelity provided by the above model would enable analysis of parachute dynamics, especially the cluster interactions leading to various modes during descent, optimisation of the loads exerted on the payload and understanding the effects on the payload trajectory.

Declarations

References

1. Duan, S.S.: A comparsion case study of dynamics analysis methods used in applied multibody dynamics, American Society for Engineering Education, 2006–1859 (2006)
2. Fallon, E.J.: Parachute dynamics and stability analysis of the queen match recovery system, AIAA Paper 91-0879 (1991) https://doi.org/10.2514/6.1991-879. https://arc.aiaa.org/doi/abs/10.2514/6.1991-879
3. Ge, Z.M., Cheng, Y.H.: Extended kanes equations for non-holonomic variable mass system. J. Appl. Mech. **49**(2), 429–431 (1982). https://doi.org/10.1115/1.3162105
4. Guglieri, G.: Parachute-payload System Flight dynamics and trajectory simulation. Int. J. Aerosp. Eng. **2012**, Article ID 182907 (2012). https://doi.org/10.1155/2012/182907

5. Heinrich, H.G., Eckstrom, D.J.: Velocity distribution in the wake of bodies of revolution based on drag coefficient. Air Force Flight Dynamics Laboratory Report ASD TDR-62-1103 (1963)

6. Henderson, D.: Euler angles, quaternions, and transformation matrices – Working relationships. National Aeronautics and Space Administration, Mission Planning and Analysis Division, Washington DC (1977)

7. Hurtado, J.E.: Analytical dynamics of variable-mass systems. J. Guid. Control Dyn. **41**(3), 701–709 (2017). https://doi.org/10.2514/1.G002917

8. Ibrahim, S.K., Engdahl, R.A.: Parachute dynamics and stability analysis NASA-CR-120326 (1974)

9. Kane, T.R., Levinson, D.A.: Dynamics, Theory and Applications. McGraw-Hill, New York (1985)

10. Ke, P., Yang, C., Sun, X., Yang, S.: Novel algorithm for simulating the general parachute-payload system: theory and validation. J. Aircr. **46**(1), 189–197 (2009). https://doi.org/10.2514/1.34240

11. Kidane, B.: Parachute drag area using added mass as related to canopy geometry. In: 20th AIAA Aerodynamic Decelerator Systems Technology Conference and Seminar (2009). https://doi.org/10.2514/6.2009-2942

12. Pal, R.S.: Modelling of helicopter underslung dynamics using Kane's method. 6th conference on Advances in Control and Optimization of Dynamical Systems ACODS. IFAC-PapersOnLine **53**(1), 536–542 (2020). https://doi.org/10.1016/j.ifacol.2020.06.090. https://www.sciencedirect.com/science/article/pii/S2405896320301099

13. Paul, J., Nalluveettil, S.J., Purushothaman, P., Premdas, M.: Combined Body Dynamics Simulation of Crew Module with Parachutes, 10th National Symposium and Exhibition on Aerospace and Related Mechanisms (2016)

14. Pei, J., Roithmayr, C.M., Barton, R.L., Matz, D.A.: Modal Analysis of a Two-Parachute System, 25th Aerodynamic Decelerator Conference. AIAA, Washington (2019)

15. Peterson, C.W., Johnson, D.W.: Reductions in parachute drag due to forebody wake effects. J. Aircr. **20**(1), 42–49 (1983). https://doi.org/10.2514/3.44826

16. Stoneking, E.: Implementation of Kane's method for a spacecraft composed of multiple rigid bodies, AIAA Guidance, Navigation (2013). And Control (GNC) Conference. https://doi.org/10.2514/6.2013-4649, https://arc.aiaa.org/doi/abs/10.2514/6.2013-4649